CHAPTER 4

THE RADIATION BUDGET

4.1 The Mean Global Energy Balance

Figure 4.1 summarizes the annual mean global energy balance for the earth-atmosphere system and indicates some of the atmospheric processes that come into play. Of the 100 units of incident solar radiation, 19 are absorbed during passage through the atmosphere: 16 in cloud-free air and three in clouds. A total of 30 units are reflected back to space: 20 from clouds, six from cloud-free air, and four from the earth's surface. The remaining 51 units are absorbed at the earth's surface. The earth disposes of this energy by a combination of infrared radiation and sensible and latent heat flux. The net infrared emission, which represents the upward emission from the earth's surface, minus the downward emission from the atmosphere, amounts to 21 units, 15 of which are absorbed in passing through the atmosphere and six of which reach space. The remaining 30 units are transferred from the earth's surface to the atmosphere by a combination of latent and sensible heat flux.

From the viewpoint of the atmosphere alone, there is a net loss of 49 units of infrared radiation (70 units emitted to space from the top of the atmosphere minus 21 units of net upward flux from the earth's surface) which exceeds by 30 units, the energy gained as a result of the absorption of solar radiation. This deficit is balanced by an influx of 30 units of latent and sensible heat from the earth's surface. Thus, in the global average, the atmosphere experiences a net radiative cooling which is balanced by the latent heat of condensation that is released in regions of precipitation, and by the conduction of sensible heat from the underlying surface. Were it not for the fluxes of latent and sensible heat, the earth's surface would have to be considerably hotter (on the order of 340 K as compared with the observed value of 288 K) in order to emit enough infrared radiation to satisfy the balance requirements for thermal equilibrium.

4.2 The First Satellite Experiment to Measure the Net Radiation

The radiation budget of net radiation, N, of the entire earth-atmosphere system is the difference between the absorbed solar radiation and the outgoing longwave radiation; therefore,

$$N = (1 - A)\, S/4 - R_{LW}$$

where A is the fraction of incoming solar energy reflected back to space (the planetary albedo), S is the incoming solar irradiance and R_{LW} is the outgoing longwave irradiance. The radiation budget equation can be written for a specific location of the earth at a given instant of time by replacing the planetary mean incoming solar radiation term (S/4) with the term S cos φ, where φ is the solar zenith angle at the location and time of interest. In this case, A is no longer the planetary albedo, but instead the bi-directional reflectance of the earth-atmosphere for that specific location and time.

The first meteorological satellite experiment flew prior to TIROS-I on the Explorer VII satellite in 1959. The experiment was devised by Suomi and Parent to provide this most basic meteorological measurement, the balance between the radiation input to the atmosphere from the sun and the radiation exiting from the atmosphere as a result of reflection and emission processes. The spatial distribution of the radiation imbalances between incoming and outgoing radiation (the net radiation) is the primary driving force of atmospheric circulation. The solar input had already been measured from ground-based and balloon borne platforms. Suomi's experiment was the first to measure the energy loss to space.

Suomi's radiometer consisted of two heat sensing detectors, one painted black to absorb radiation at all wavelengths, and the other painted white to reflect the shortwave sun's energy and

thereby absorbed only earth emitted radiation. Thus, Suomi was able to differentiate between the energy leaving the earth's atmosphere due to reflected sunlight (provided by the difference between the radiation sensed by the black and white sensors) and that emitted by the earth and atmosphere (the radiation measured by the white sensor).

In a short time after exposure to various radiative components involving the direct solar flux, solar flux reflected by the earth and atmosphere (shortwave), and thermal infrared flux emitted by the earth and atmosphere (longwave), each sensor achieves radiative equilibrium. It is assumed that the absorptivity of the black sensor a_b is the same for shortwave and longwave radiation. However, the absorptivity of the white sensor for shortwave and longwave radiation are given by a_w^S and a_w^L, respectively. Let the temperatures measured by the black sensors and white sensors be T_b and T_w, respectively. On the basis of the Stefan-Boltzmann and Kirchhoff laws, radiative equilibrium equations for both sensors may be expressed by

$$4\pi r^2 a_b \sigma T_b^4 = \pi r^2 a_b (E_o + E_S + E_{IR})$$

and

$$4\pi r^2 a_w^L \sigma T_w^4 = \pi r^2 [a_w^S (E_o + E_s) + a_w^L E_{IR}] .$$

These two equations show that the emitted energy per unit time is equal to the absorbed energy per unit time, where $4\pi r^2$ and πr^2 represent the emission and absorption areas, respectively, for the two spherical sensors each with a radius r. The irradiances of the reflected shortwave, longwave radiation, and direct solar are denoted by E_S, E_{IR}, and E_O, respectively.

Upon solving the sum of the shortwave and the longwave irradiances, we obtain

$$E_o + E_S = [4 \sigma a_w^L / (a_w^L - a_w^S)] (T_b^4 - T_w^4)$$

and

$$E_{IR} = [4 \sigma /(a_w^L - a_w^S)] (a_w^L T_w^4 - a_w^S T_b^4)$$

The direct solar irradiance E_O can be evaluated from the solar constant, which is specified prior to the experiment.

In order to convert the measured irradiances into radiances emitted and reflected by the earth, one must consider the solid angle Ω which the earth subtends to the satellite sensor. For a satellite at height h above the earth surface, it can be shown from simple geometric considerations that

$$\Omega = 2\pi [1 - (2Rh + h^2)^{1/2} / (R + h)],$$

where R represents the radius of the earth. Then the radiance I is given by

$$I = E/\Omega ,$$

since the spherical sensor is equally sensitive to radiation from all directions, eliminating the cosine dependence with respect to angle of incidence.

4.3 The Radiation Budget

The circulation of the earth's atmosphere and oceans can be thought of as being powered by a heat engine. The shortwave radiation from the sun provides the fuel supply while the infrared radiation heat loss to space from the earth's surface and atmosphere is the exhaust. The engine is throttled, to a large extent, by storms and ocean disturbances associated with the transformation of radiative heat to latent and sensible heat.

The distribution of sunlight with latitude is responsible for our major climatic zones (Tropical, Temperate and Polar). The composition of the atmosphere and the characteristics of the earth's surface also play an important role in the climate of local regions such as deserts. Small changes in the sun's radiation or the terrestrial radiation due to natural or man induced changes in atmosphere and surface composition might lead to major variations in our climate.

The net radiation for the earth may vary through the year in accordance with earth-sun distance since S varies 6% between January and July. However, when integrated over an entire year, the net radiation must be near zero, otherwise long-term climatic changes would occur. On the planetary and regional scales, clouds play the major role in upsetting the normal state of radiation balance. The importance of clouds in the radiation balance is demonstrated in Figure 4.2. It shows the relation between the longwave radiation to space as a function of cloud amount and height for a standard atmospheric temperature and moisture condition. Also shown is the absorbed solar radiation as a function of cloud amount. The longwave radiation to space decreases with increasing cloud cover and cloud height because cloud temperatures are considerably lower than the earth's surface and they decrease with cloud elevation. However, clouds are also good reflectors of solar radiation and consequently the global albedo increases the absorbed solar energy decreases with increasing cloud cover since clouds generally have higher albedos than the earth's surface.

Figure 4.3a displays the globally averaged monthly mean values of various radiation budget parameters from July 1975 through December 1976. The annual cycles seem to repeat, as the values observed during July 1976 through December 1976 are nearly the same as those observed one year earlier. The albedo and longwave radiation cycles are nearly 180 degrees (six months) out of phase, possibly the result of two phenomena. The variation of the longwave radiation with time is the first consideration. In the Northern Hemisphere, the heating and cooling rates correspond to that expected for land surfaces, so outgoing longwave radiation reaches a maximum in July and a minimum in December. In the Southern Hemisphere, it is dominated by sea surfaces, so only a weak cycle is observed because the seasonal variation of sea-surface temperature is negligible. Therefore, the variation of the globally averaged longwave radiation with time is dominated by the Northern Hemisphere. During the months when the longwave radiation is at a minimum, the snow and ice cover and thus albedo in the Northern Hemisphere are close to a maximum. When the longwave radiation is at a maximum, the snow and ice cover are greatly reduced. A second consideration of equal importance is the annual cycle of cloudiness. There tends to be more cloudiness in the Northern Hemisphere winter than in the Southern Hemisphere winter. This tends to increase the albedo and decrease the longwave radiation. The opposite effect occurs around June when the cloudiness is least. It is uncertain at this time which of the two effects discussed above is the dominant cause of the variations of the longwave radiation and albedo.

As shown in Figure 4.3b, the variation with time in the absorbed solar radiation (incoming minus reflected solar radiation) appears to be principally dependent upon the variation of the incoming solar radiation. The annual variation of the incoming solar radiation about its mean value is ± 11.4 W m^{-2}, while the variation of the net energy about its mean value is only about ± 7.6 W m^{-2}, both nearly in phase with each other. If the earth were in a perfectly circular orbit around the sun so that there were no variations in the incoming radiation due to variations in the earth-sun distance, then the variation in absorbed solar radiation would be dominated by variation in the reflected energy. This would cause the phase of the absorbed solar radiation to be shifted about 180 degrees from that observed. Minima and maxima of the absorbed solar radiation correspond to maxima and minima, respectively, of the reflected radiation. Since the net radiation is the difference of the absorbed solar radiation and the outgoing longwave radiation, which are nearly 180 degrees out of phase with each other, the variation in the net radiation has an amplitude exceeding that of the absorbed and outgoing components and nearly the same phase as the absorbed solar radiation.

4.4 Distribution of Solar Energy Intercepted by the Earth

The solar irradiance at the top of the atmosphere depends strongly on the zenith angle of the sun and much less strongly on the variable distance of the earth from the sun. If the zenith angle, θ, is assumed to be constant over the solid angle subtended by the sun, the irradiance on a horizontal surface varies as cos θ. The zenith angle depends on latitude, time of day, and the tilt of the earth's axis to the rays of the sun (celestial longitude). The mean value of the earth-sun distance, R_{es}^{m}, is about 1.495 x 10^{11} metres. The minimum distance occurs on about 3 January during perihelion and is 1.47 x 10^{11} metres; the maximum distance occurs on about 5 July during aphelion and is 1.52 x 10^{11} metres.

The total energy received per unit area per day, called insolation and denoted by Q_O, may be calculated by integrating over the daylight hours as follows:

$$Q_o = S\,(R_{es}^{m} / R_{es})^2 \int_{\text{sunrise}}^{\text{sunset}} \cos\theta \, dt$$

where S represents the mean solar irradiance.

Figure 4.4 shows the results of evaluating Q_O for a variety of latitudes and dates. The maximum insolation is shown to occur at summer solstice at either pole. This is the result of the 24 hour solar day. The maximum in the Southern Hemisphere is higher than in the Northern Hemisphere because the earth is closer to the sun during the northern winter than during the northern summer.

4.5 Solar Heating Rates

Absorption of solar radiation by various gases results in heating in the atmosphere. Heating rate variation with atmospheric pressure is derived in a straightforward manner from net flux considerations. Starting with a plane parallel absorbing and scattering atmosphere, let the differential thickness within the atmosphere be Δz and the monochromatic downward and upward irradiances at wavelength λ be $E_\lambda^{\downarrow}$ and $E_\lambda^{\uparrow}$ respectively. The net monochromatic irradiance (downward) at a given altitude is then given by

$$E_\lambda (z) = E_\lambda^{\downarrow} (z) - E_\lambda^{\uparrow} (z) .$$

Because of absorption, the net monochromatic irradiance decreases from the upper levels to the lower levels. The loss of net monochromatic irradiance or the divergence for the differential layer is given by

$$\Delta E_\lambda (z) = E_\lambda (z) - E_\lambda (z + \Delta z)$$

From the definition of absorption, we also have

$$\Delta E_\lambda (z) = -E_\lambda^{\downarrow} (z + \Delta z)\, a_\lambda (\Delta z)$$

Energy conservation requires that the absorbed energy has to be used to heat the layer, so that

$$\Delta E_\lambda (z) = -\rho\, C_p\, \Delta z\, dT / dt$$

where ρ is the air density in the layer, C_p is the specific heat capacity at constant pressure, and t is the time. Combining these expressions yields the heating rate

$$dT/dt = E_\lambda^{\downarrow} (z + \Delta z)\, a_\lambda (\Delta z) / (\rho\, C_p\, \Delta z)$$

The heating rate is explicitly a function of the spectral interval; to derive a total heating rate it is necessary to sum the spectral intervals where the absorption coefficient is non zero.

Figure 4.5 shows the solar heating rate profile up to 30 km using two different atmospheric profiles (mid latitude winter and tropical) for a clear atmosphere with the sun directly overhead. Effects of absorption by O_3, H_2O, O_2, and CO_2, multiple scattering by molecules, and the ground reflection are accounted for. The maximum heating rate is seen to occur at 3 km and have a value as high as 4 degrees Centigrade per day. The heating rate decreases drastically with increasing altitude due to the decrease of water vapour concentration and reaches a minimum at roughly 15 km. Above 20 km, the increased solar heating is caused by the absorption of ozone, which has a maximum concentration at about 25 km.

4.6 Infrared Cooling Rates

Emission (absorption) of infrared radiation by various gases produces a cooling (heating) effect in the atmosphere. In the same way that solar heating is a function of the net transfer of radiation in the downward direction (as solar radiation enters from the top of the atmosphere), infrared cooling is a function of the net transfer of radiation in the upward direction (as thermal radiation can be thought of as originating from the earth surface). An analogous derivation yields

$$dT/dt = - (\Delta\, E_\lambda / \Delta z) / (\rho\, C_p)$$

where ΔE_λ represents the net loss of irradiance in the layer Δz.

A calculation of infrared cooling rates as a function of height in the clear tropical atmosphere is illustrated in Figure 4.6. In the lower 2 km the most important band influencing the cooling is the water vapour continuum. This is due to the rapid increase in the temperature and the partial pressure of water vapour as one gets closer to the surface. Above 5 km the water vapour continuum contributes very little to the infrared cooling rate. In the middle and upper troposphere, absorption is mostly in the water vapour rotational band. A large increase in ozone concentration between 18 and 27 km results in a strong heating. Above 30 km the cooling rate increases rapidly due to the CO_2 15 μm and O_3 9.6 μm bands.

4.7 Radiative Equilibrium in a Gray Atmosphere

The concept of a balanced atmosphere that transfers energy only through radiative transfer (no conduction or convection) is useful to derive some of the characteristics of the earth atmosphere. Given a heated surface and a gray atmosphere in balance, one can write that the net irradiance at any level is constant, since

$$d/dz\, [E^{\uparrow} - E^{\downarrow}] = \rho\, C_p\, dT/dt = 0 \qquad (1)$$

The irradiance going up through a layer can be written

$$d/d\chi^*\, [E^{\uparrow}] = E^{\uparrow} - \pi B \qquad (2)$$

and similarly for the irradiance going down through a layer

$$-d/d\chi^*\, [E^{\downarrow}] = E^{\downarrow} - \pi B \qquad (3)$$

where πB is given by Stefan's Law and χ^* is an effective optical depth integrated from the top of the atmosphere down over all angles in the hemisphere. Adding equations (2) and (3) yields

$$d/d\chi^* [E^{\uparrow} - E^{\downarrow}] = E^{\uparrow} + E^{\downarrow} - 2\pi B = 0 , \quad (4)$$

and subtracting (2) - (3) gives

$$d/d\chi^* [E^{\uparrow} + E^{\downarrow}] = [E^{\uparrow} - E^{\downarrow}] = \Delta = \text{const.} \quad (5)$$

or using (4)

$$\pi B = \Delta \chi^*/2 + \pi B_o . \quad (6)$$

The boundary conditions are such that there is no downward irradiance at the top of the atmosphere

$$E^{\downarrow} (\text{top}) = 0 , \text{ and}$$

$$\chi^* (\text{top}) = 0 ,$$

and at the bottom of the atmosphere the upward irradiance must be dictated by Stefan's Law applied to the surface temperature

$$E\uparrow (\text{bot}) = \sigma T (\text{sfc})^4 , \text{ and}$$

$$\chi^* (\text{top}) = \chi^* (\text{tot})$$

where $\chi^*(\text{tot})$ is the effective optical depth of the total atmosphere. Then we find that

$$\pi B = \Delta (\chi^*+1) / 2 \text{ and} \quad (7)$$

$$\pi [B (\text{sfc}) - B (\text{bot})] = \Delta/2 \quad (8)$$

The function πB is plotted against χ^* in Figure 4.7. At the surface there is a discontinuity in temperature, as dictated by Eq. (8). Combining Eq. (7) and (8)

$$\pi B (\text{sfc}) = \Delta (\chi^* (\text{tot}) +2) /2 . \quad (9)$$

Or written more simply in terms of temperature

$$T (\text{sfc})^4 - T (\text{top})^4 = T (\text{bot})^4 \quad (10)$$

and

$$\chi^* (\text{tot}) = [T (\text{sfc})^4 / T (\text{top})^4] - 2 . \quad (11)$$

When the atmosphere effective optical depth is large, the surface temperature is enhanced, as expected by the greenhouse effect. The optical depth of an atmosphere depends on the concentration of H_2O, CO_2, and O_3. In the case of H_2O the concentration may increase with increasing temperature (through evaporation) and thus creating positive feedback for the greenhouse effect. This effect is very noticeable on Venus, which exhibits "runaway greenhouse effect."

Figure 4.8 is the equivalent diagram in terms of temperature and height to Figure 4.7. The lower part of the atmosphere shows a very steep lapse rate of temperature that is unstable with respect to vertical motion; in a more realistic atmosphere, convection would tend to establish a

mean adiabatic lapse rate. Air from near the surface would tend to rise along the mean adiabatic lapse rate of -6 K / km and intersect with the radiative equilibrium curve at a height of about 10 km or near the tropopause. In mid-latitudes the tropopause divides the troposphere where convection is dominant from the stratosphere where radiative transfer is dominant.

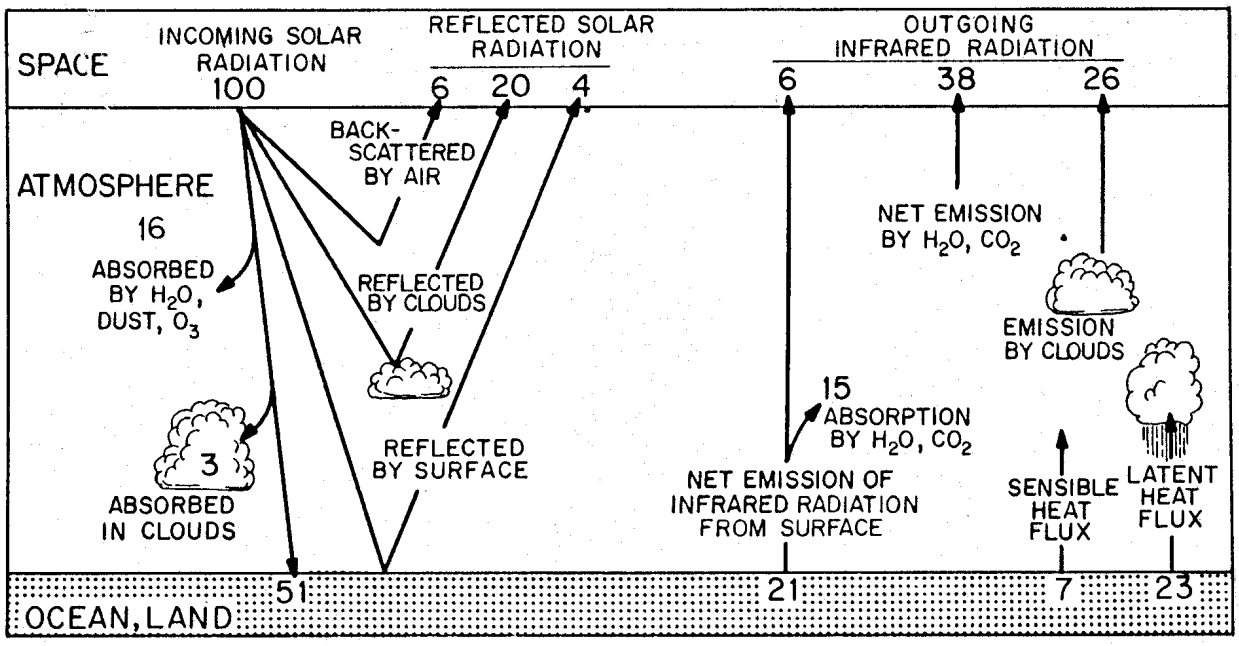

Figure 4.1: The annual mean global energy balance for the earth-atmosphere system. (Numbers are given as percentages of the globally averaged solar irradiance incidence upon the top of the atmosphere.)

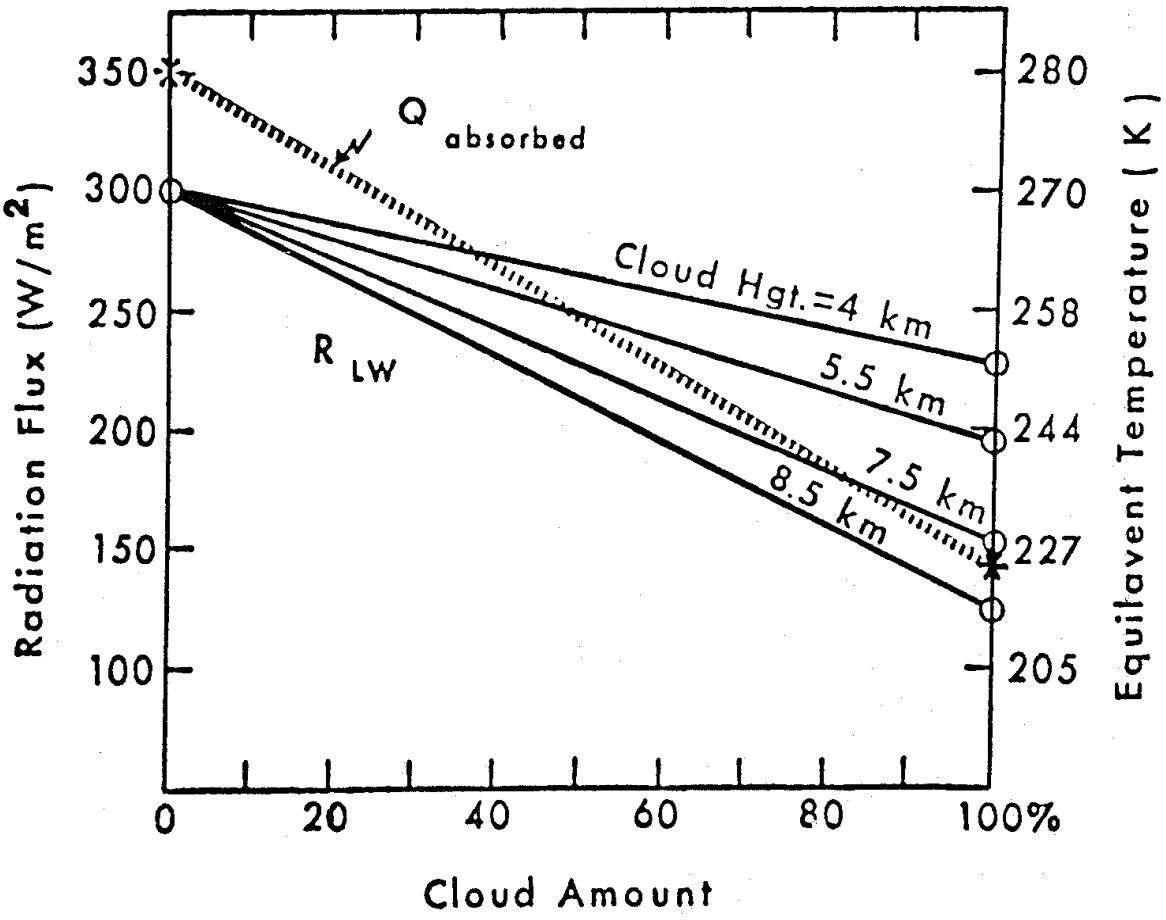

Figure 4.2: Longwave radiation to space, R, and absorbed solar radiation, Q, as a function of cloud amount.

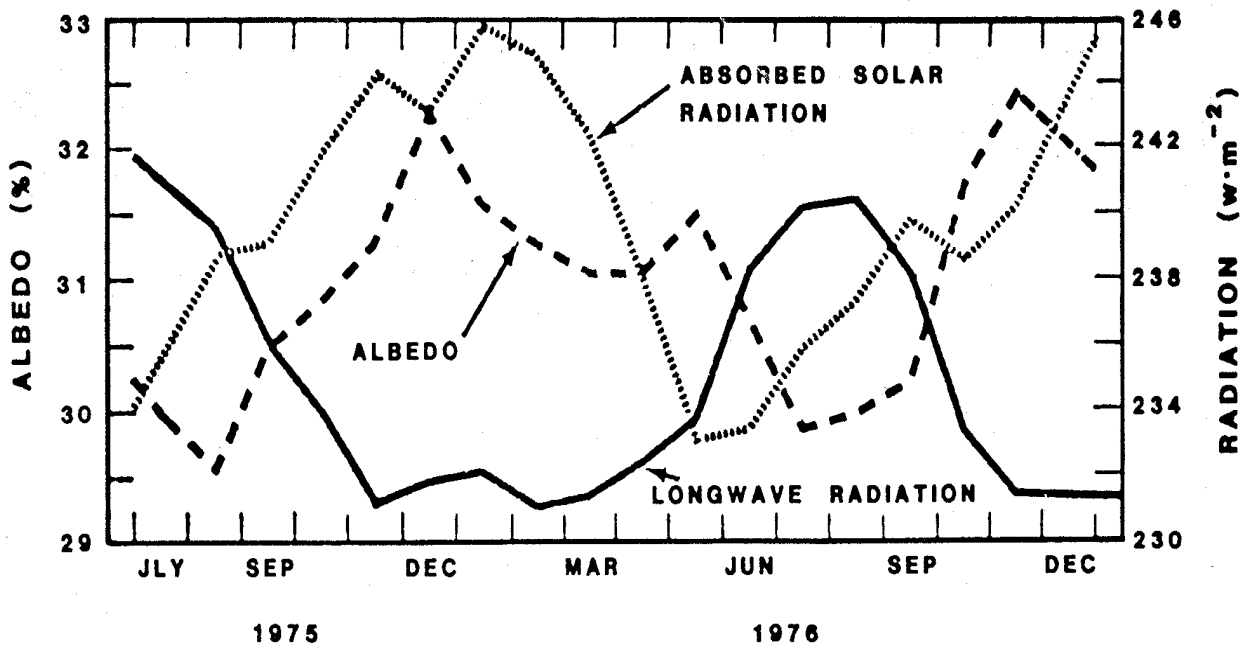

(a)

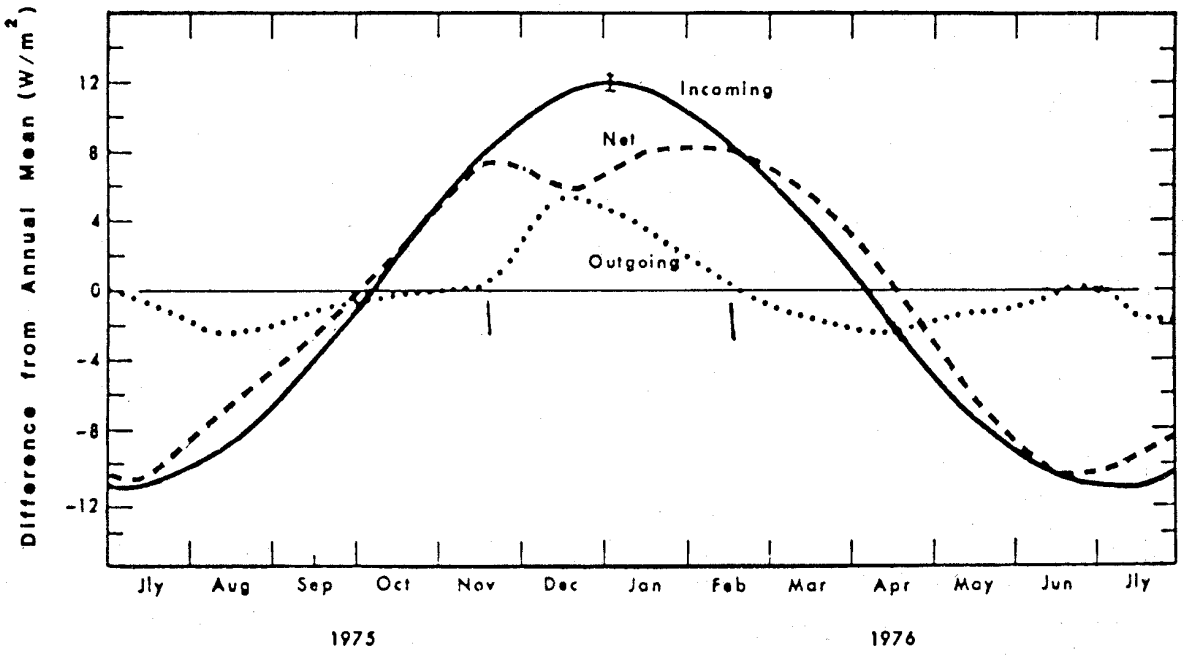

(b)

Figure 4.3: (a) Globally averaged monthly mean values of radiation budget parameters. (b) Variation in time with respect to an annual mean of net, incoming, and outgoing radiation.

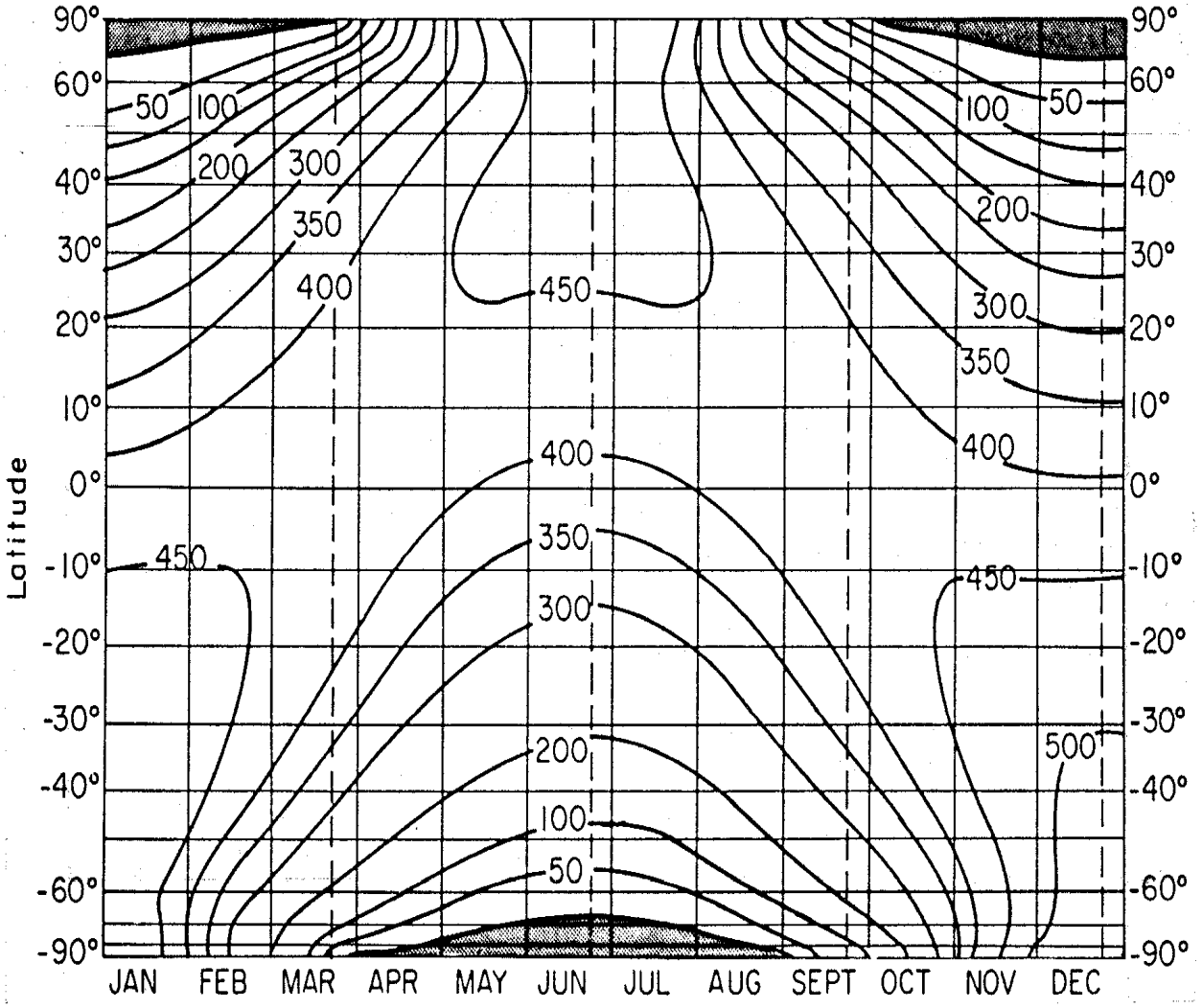

Figure 4.4: Daily solar insolation in W/m^2 incident on a horizontal surface at the top of the atmosphere as a function of latitude and date (adapted from Milankovitch, 1930).

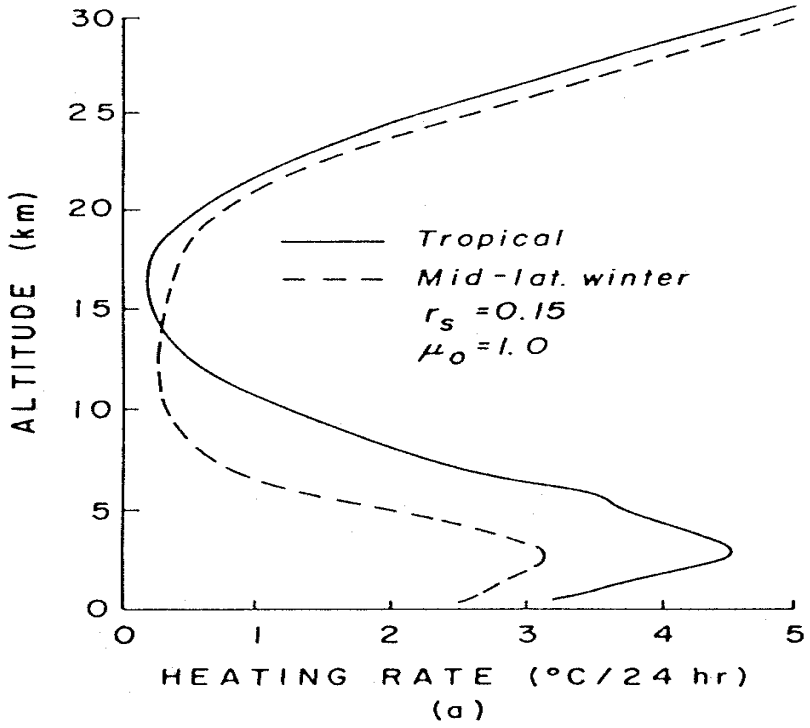

Figure 4.5: Solar heating rate calculated from atmospheric profiles appropriate for tropical and mid latitude winter conditions (Liou, 1980).

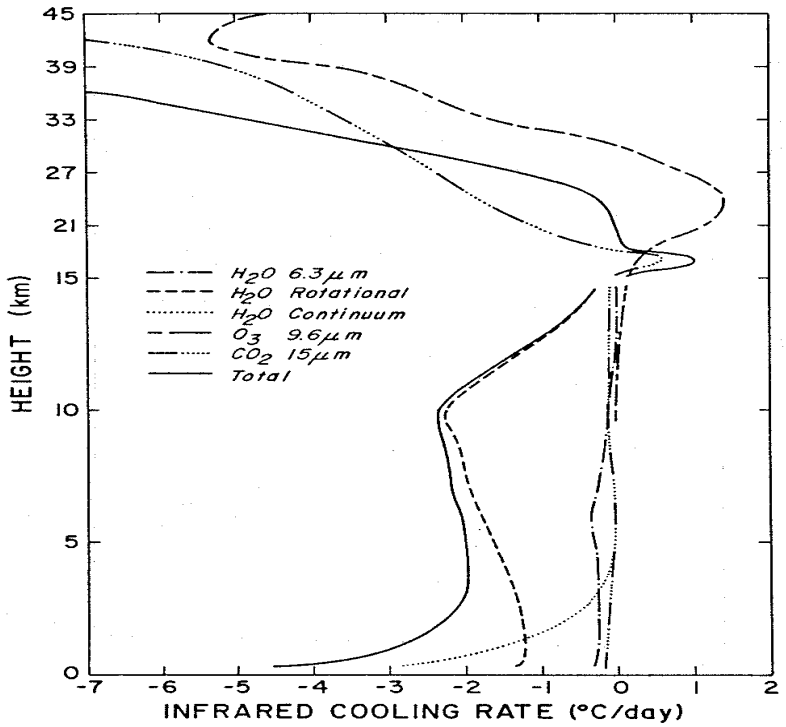

Figure 4.6: Calculation of total and partial cooling rates with an atmospheric profile appropriate for clear tropical conditions (after Roewe and Liou, 1978).

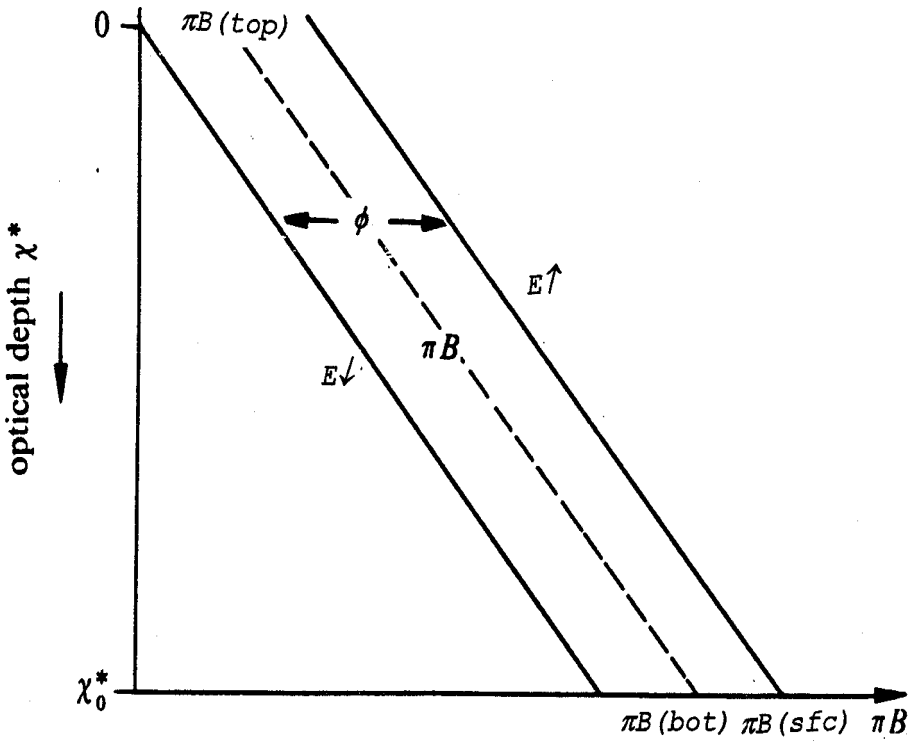

Figure 4.7: Upward E↑ and downward E↓ irradiance and emitted radiance from a given layer πB (given by Stefan's Law) plotted as a function of effective optical depth χ* in an atmosphere in radiative equilibrium.

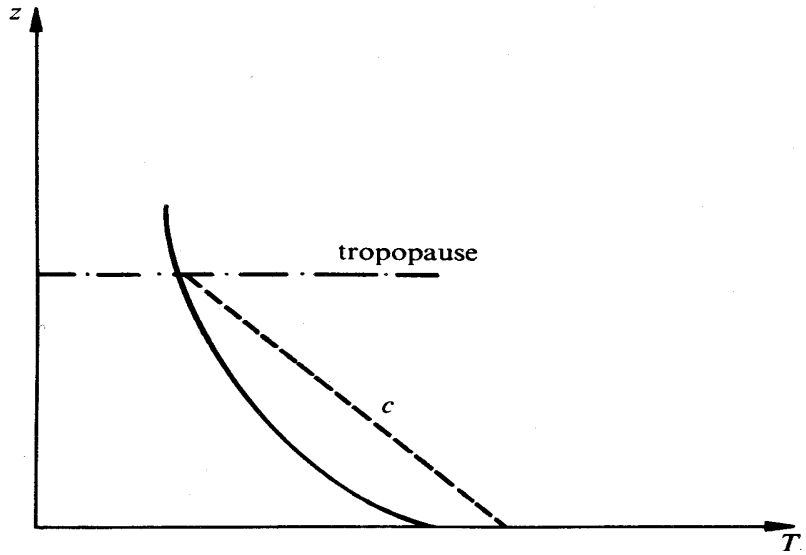

Figure 4.8: Radiative equilibrium temperature plotted versus altitude z. The line c indicates an adiabatic lapse rate of -6 K / km originating from the surface temperature.